6th Fatigue Design conference, Fatigue Design 2015

Rotor Design Optimisation through Low Cycle Fatigue Testing

C. Schayes[a,b], J.-B. Vogt[a,*], J. Bouquerel[a], F. Palleschi[b]

[a]UMET – UMR ENSCL/ Université de Lille/CNRS 8207, team Métallurgie Physique et Génie des Matériaux, Université de Lille, Bâtiment C6, 59655 Villeneuve d'Ascq, France
[b]Valeo Engine Electrical Systems, 2 rue André Boulle, 94046 Créteil, France

Abstract

The current work aims at modifying the rotor geometry to improve the alternator performance. For that purpose, the fatigue behaviour of the material needs to be defined. Experimental tests were conducted on the Fe-3Si steel constituting the rotor. It is shown that this material hardens under cyclic loadings and TEM observations revealed unusual damage mechanisms. From the experimental LCF tests, the material parameters needed for FEA and the fatigue resistance law have been defined. The FEA results were validated on smooth and notch samples. Finally, the rotor design is modified which enables a light-weighting of the magnet or an increase of the torque value depending on the considered rotor and purpose.

Keywords: cyclic accommodation; fatigue rsistance; fatigue failure; dislocatios structure; modelling

1. Introduction and context

With the unusual missions related with the stop&start function of new starter-alternator such as designed by Valeo, fatigue damage is suspected to limit the performance of some components of the machine. The rotor of these machines consists of a stack of thin steel sheets of Fe-3Si. Up to now, the rotor design is based on the Haigh diagram [1] construction and no failure has been encountered. This good situation is however not very acceptable because the rotor is probably oversized. In addition, the improvement in the electro-technical properties suggests promoting small controlled cyclic plastic deformation. Therefore the fatigue behaviour of the Fe3Si steel i.e. stress

* Corresponding author. Tel.: +33 (0) 320 43 40 35; fax: +33 (0) 320 43 65 91.
  E-mail address: jean-bernard.vogt@ensc-lille.fr

response to strain cycling, fatigue resistance, cyclic plasticity accommodation and damage mechanisms are of prime interest but nearly absent in the literature.

The objective of the present paper is to bring the missing knowledge in the low cycle fatigue behaviour of the Fe3Si steel provided in the form of thin sheet. Both identification of fatigue mechanism and assessment of data base implemented in a finite element analysis will be considered. This must result in a new rotor design that improves the functional performance and decrease the weight of the machine.

Nomenclature

$\Delta\varepsilon_t$	Total strain variation
$\dot{\varepsilon}$	Strain rate
$\Delta\sigma/2$	Stress amplitude
FEA	Finite Element Analysis
LCF	Low Cycle Fatigue

---

2. Experimental work

2.1. Material

The material of the study is a non-oriented silicon steel with the chemical composition given in Table 1.

Table 1. Chemical composition of Fe-3Si (wt%)

Elements	C	Mn	P	Si	S	Al	Fe
wt%	0.003	0.109	0.011	2.884	0.004	0.448	Bal.

The material exhibits a ferritic structure (Fig. 1 (a)) with a wide grain size distribution (Fig. 1 (b)). The average grain size determined by the intercept method is 75 µm. The material has been provided in thin sheet, 350 µm in thickness, which corresponds to a thickness of 4 to 5 grains. The grains are not randomly oriented but rather show a [1 1 1] // ND fibres, no details regarding the rolling conditions have been given by the supplier.
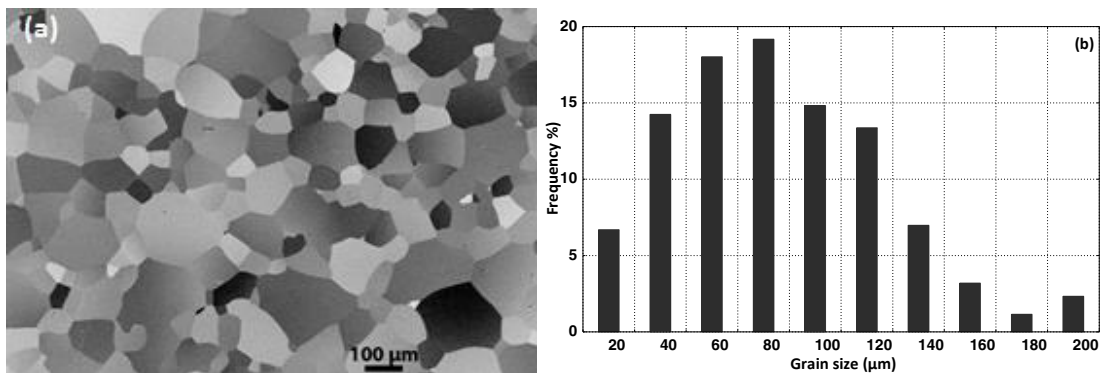

Fig. 1. (a) Microstructure of the Fe-3Si steel; (b) Grain size distribution of the Fe-3Si steel.

The tensile curve of the material is shown in Fig. 2 and the mechanical properties are detailed in Table 2. Fe-3Si is a soft and ductile material with a Young modulus E=186 GPa and an elongation to fracture A=28%.
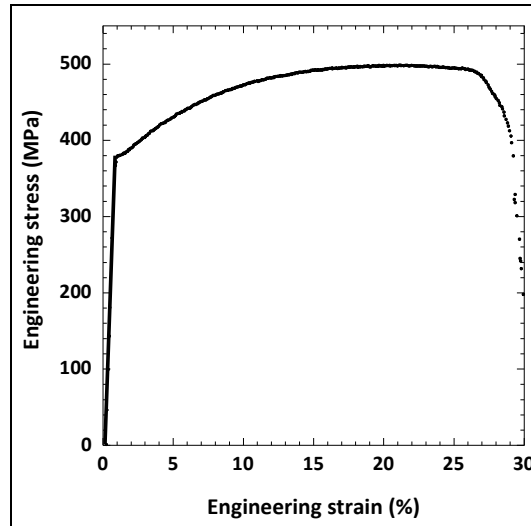

Fig. 2. Tensile curve of the Fe-3Si steel at room temperature, $\dot{\varepsilon} = 4.10^{-3}s^{-1}$

Table 2: Mechanical properties of the Fe-3Si steel at room temperature

Young modulus E (GPA)	Yield strength YS (MPa)	Ultimate tensile strength UTS (MPa)	Elongation A (%)	Uniform elongation $A_{u (\%)}$	Hardness HV0.5
186	367	499	28	20	180

2.2. Mechanical tests

2.2.1. Low cycle fatigue (LCF)

LCF tests were performed on a MTS servo-hydraulic machine under total axial strain control $\Delta\varepsilon_t$ ranging from 0.3 % to 1 %. A push-pull mode (R_ε=0), a triangular wave form, and a constant strain rate of 10^{-2} s^{-1} were employed. Flat specimens with 12 mm gauge length and 6 mm width were used (Fig. 3.). With specimen size following standard, mechanical tests in push-pull mode is not possible due to the thickness of the steel sheet. In addition to specimen size modification, the specimens were inserted in an anti-buckling system. Their surfaces were finely electro-polished before testing. Strain was measured by means of an extensometer of 8 mm gauge length. The fatigue life is defined as the number of cycles leading to a drop of 25% of the tensile stress thereby taking the mid-life pseudo stabilized hysteresis loop as reference.
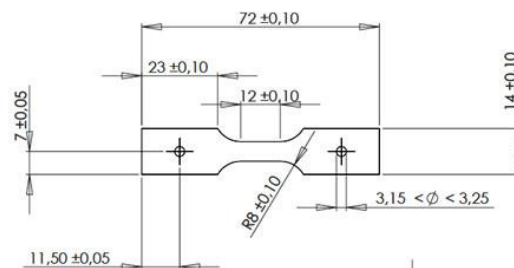

Fig. 3. Specimen dimension for LCF tests

The evolution of the stress amplitude with the number of cycles and with the life fraction of the Fe-3Si steel is reported, respectively, in Fig. 4 (a) and Fig. 4. (b). It is characterized by a very short transient period (of about 10 cycles) followed by a rapid hardening stage and then a moderate rate hardening stage. For the test performed at $\Delta\varepsilon_t$=0.3%, the evolution is almost constant with a stress value lower than the yield stress. For the higher strain amplitudes test ($\Delta\varepsilon_t > 0.5\%$), the transition between the high and low hardening rate periods represents about 30% of the fatigue life. Figure 4b shows that the hardening is very strong at the beginning of the fatigue life and then attenuates for the major part of the life.

The hardening of the material is beneficial in terms of stress response to cyclic strain. This means that localized plastic straining in the final component may be acceptable.
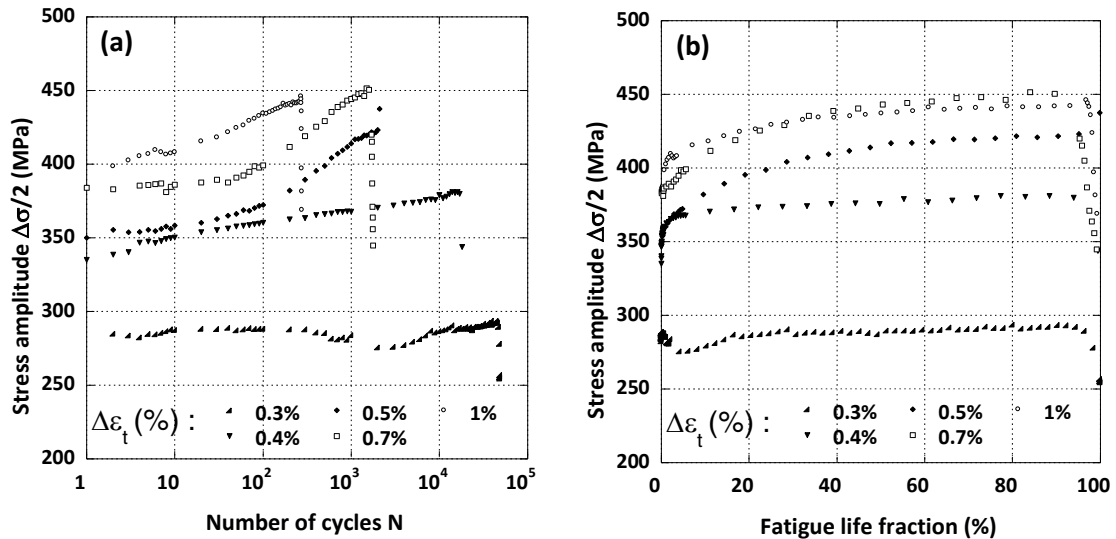

Fig. 4. Evolution of the stress amplitude of the Fe-3Si steel with the number of cycles (a) and with the fraction of lifetime (b)

The plastic, elastic and total strain variations were evaluated from hysteresis loop analysis. These values taken at 70% of fatigue life of each test are plotted against the number of cycles to failure for each sample in Fig. 5. The fatigue resistance fits well the Manson-Coffin equation defined in equation (1), where $\Delta\varepsilon_{pa}$ is the plastic strain variation, K_p and C_p are, respectively, coefficient and exponent of resistance to fatigue and Nr the number of cycles at failure. This law is thus suitable for fatigue life prediction from strain measured in FEA.

$$\Delta\varepsilon_{pa}=K_p(N_R)^{Cp} \quad \text{with } K_p = 27.3 \ C_p = -0.77 \tag{1}$$
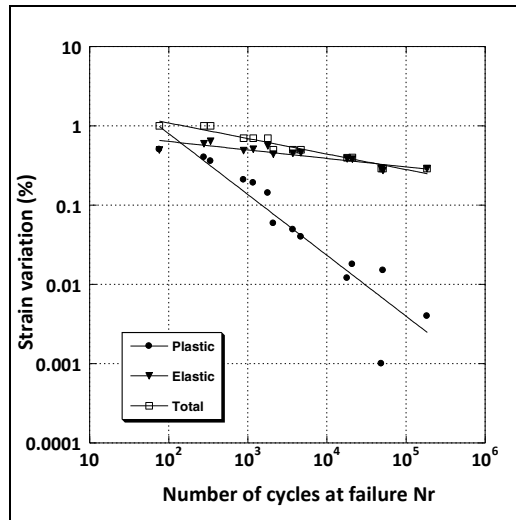
Fig. 5. Fatigue resistance as a function of plastic, elastic and total strains of the Fe-3Si steel.

2.2.2. Cyclic tests on notched samples

Additional cyclic tests were conducted on notched samples for comparison with FE results. Notched samples are little studied in LCF, as they are classically considered for fatigue crack propagation study.

The notch radius of the samples is chosen in order to be the closest to the radius found in the geometry of the industrial rotor. The geometry of the sample is defined in Fig.6. These samples were subjected to fatigue tests with control of the force; the test parameters are detailed in table 3.

Table 3: Parameters of the cyclic tests conducted on notched specimen

Applied force	Signal	Frequency
300 à 700N	Triangular	2 Hz

The number of cycles to failure is recorded for each level of studied force. The results obtained are shown in Fig. 7.
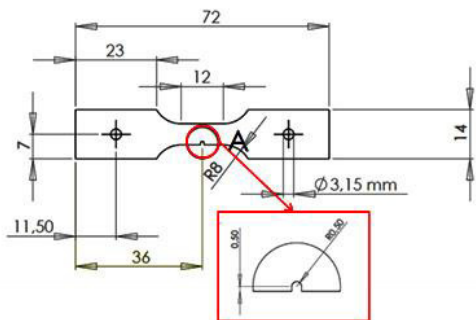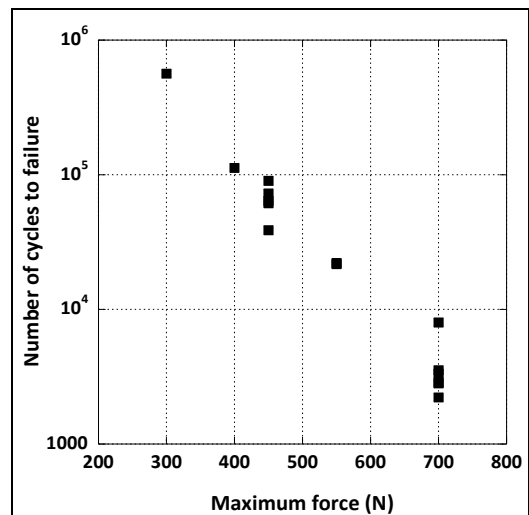

Fig. 6. Geometry of the notched samples.

Fig. 7. Experimental fatigue life of the notched specimens

2.2.3. Microstructural aspects of fatigue damage

2.2.3.1. Crack initiation and propagation

SEM observations of the surface of the polished LCF samples revealed an effect of the strain variation on crack initiation sites. Indeed, below $\Delta\varepsilon_t$=0.7%, crack initiation is mainly transgranular (Fig. 8.), and above $\Delta\varepsilon_t$=0.7%, crack initiation is intergranular (Fig. 9.). At $\Delta\varepsilon_t$=0.7%, mixed crack initiation mode is observed. Regarding crack propagation, it is brittle for every tested strain variation (Fig. 10.).
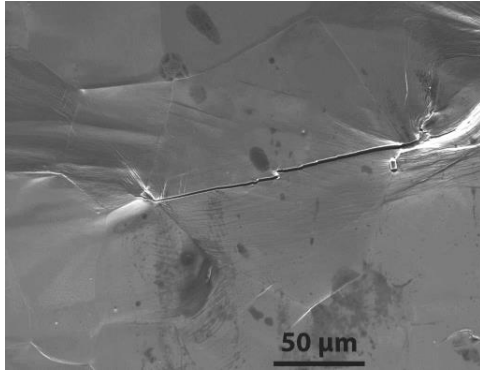
Fig. 8. SEM image of a sample after fatigue failure at $\Delta\varepsilon_t$=0.5% showing transgranular crack initiation
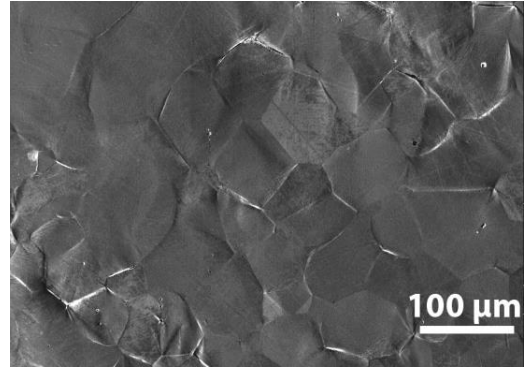
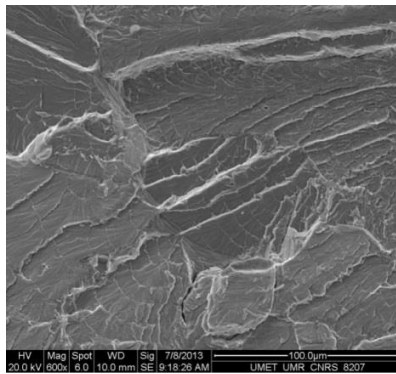Fig. 9. SEM image of a sample after fatigue failure at $\Delta\varepsilon_t$=1% showing intergranular crack initiation

Fig. 10. SEM image of a sample after fatigue failure at $\Delta\varepsilon_t$=1% showing brittle crack propagation

2.2.3.2. Dislocation structure

Dislocation structures were observed as well by TEM as by SEM-ECCI. Observation of dislocation structures have been carried out on fractured specimen as a function of the applied strain (Fig. 11.).
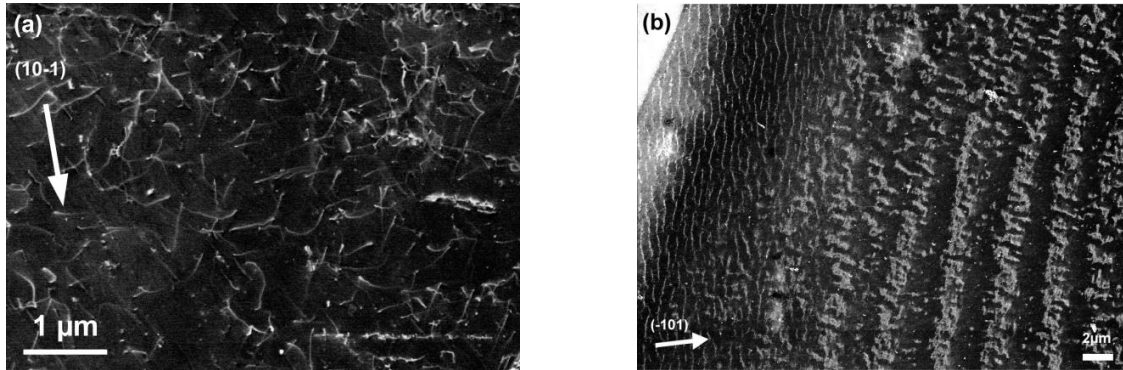
Fig.11. Dislocation structure observed by SEM-ECCI at a) $\Delta\varepsilon_t$=0.5% and b) $\Delta\varepsilon_t$=1%

The transition at $\Delta\varepsilon_t$=0.7% is also observed. Indeed, below this transition strain, short isolated dislocations are observed and 2 slip systems are activated (Fig. 11. a). Above $\Delta\varepsilon_t$=0.7%, well organised dislocation structures are observed, with a wall structure near grain boundaries and a vein structure in the grain interior (Fig. 11. b).

The formation of dislocation structures, as $\Delta\varepsilon_t$ increases, proceeds gradually to form an organised wall structure without ever forming a cell structure as it could be expected for ferritic steels [2]. More details regarding the plasticity mechanisms of this material are given in [3] and in [4].

Thereby, whether a component made of this steel is loaded in the low strain regime or the high strain regime can be determined by the developed dislocation structure but also by the crack initiation sites.

3. Numerical Investigation

3.1. Model definition

To compute stress/strain state of the specimen subjected to cyclic loading, finite element analysis is used with the kinematic model of Armstrong and Frederick (1966) [5] combined with cyclic hardening, generally referred as Chaboche nonlinear kinematic hardening, and is defined in equation (2).

$$\dot{X} = \frac{2}{3} C \dot{\varepsilon}^p - \gamma X \dot{p} \tag{2}$$

With $\dot{X}$, the nonlinear kinematic hardening of Armstrong-Frederick, $\dot{p}$ the cumulative plastic strain rate, C and γ material parameters. The integration of this law in the uniaxial domain leads to the following equation (3):

$$\frac{\Delta X}{2} = \frac{C}{\gamma} tanh\left(\gamma \frac{\Delta\varepsilon_P}{2}\right) \tag{3}$$

With $\Delta\varepsilon_p$, the plastic strain variation.

In this study, isothermal conditions and independent of the strain rate enable the writing of $\Delta\sigma$ in the form of $\Delta X+2k$. Then, in the stabilized regime, the following expression is obtained (4):

$$\frac{\Delta\sigma}{2} - k = \frac{C}{\gamma} tanh\left(\gamma \frac{\Delta\varepsilon_p}{2}\right) \tag{4}$$

With k the elastic limit of the stabilized regime.
By adding several hardening models, it is possible to improve the model; the following equation is finally obtained (5).

$$\frac{\Delta\sigma}{2} - k = \sum_{i=1}^{M} \frac{C_i}{\gamma_i} tanh\left(\gamma_i \frac{\Delta\varepsilon_p}{2}\right) \tag{5}$$

C_i and γ_i are material parameters.

Experimental hysteresis curves are processed to determine k (fig.12) and the C_i and γ_i parameters were obtained by adjustment of the curve plotted in fig.13 [5].
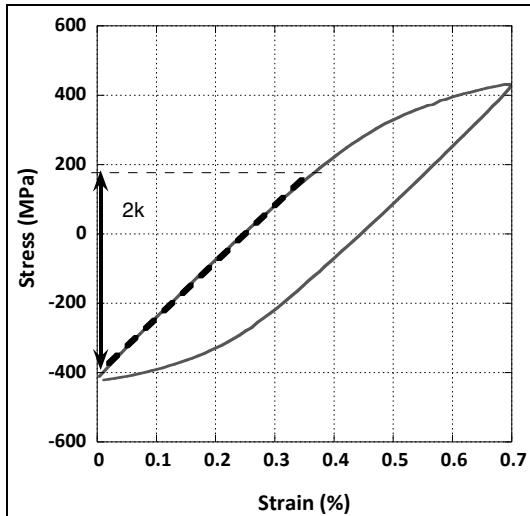

Fig.12. Determination of the stabilized elastic limit from stabilized hysteresis curves (taken at 70% of fatigue life)
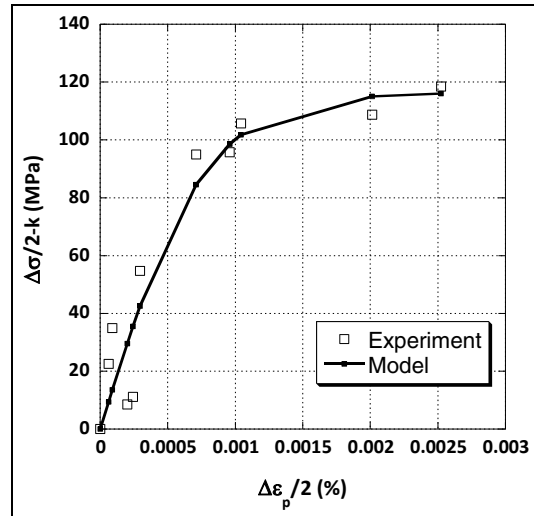
Fig.13. Identification of the parameters C_i and γ_i. Each point represents a fatigue test and the curve is obtained by adjustment

3.2. Validation of the model

3.2.1. Life estimation on smooth samples

First, this model must be validated on simple geometry. For that purpose, FEA on a rectangle of the same dimensions of the fatigue samples subjected to cyclic strain were conducted with the software Ansys. Hysteresis curves (stress vs strain) obtained by FEA and by experiment plotted in Fig. 14 show good agreement. The error between experimental and modelled plastic strain is less than 11% for every strain variation. It is low enough to use the Manson-Coffin law defined in equation (1) to estimate fatigue life from FEA. The results are presented in Fig. 15 and validate the use of this law for life prediction as the error is less than 20% which is acceptable when considering experimental scattering.
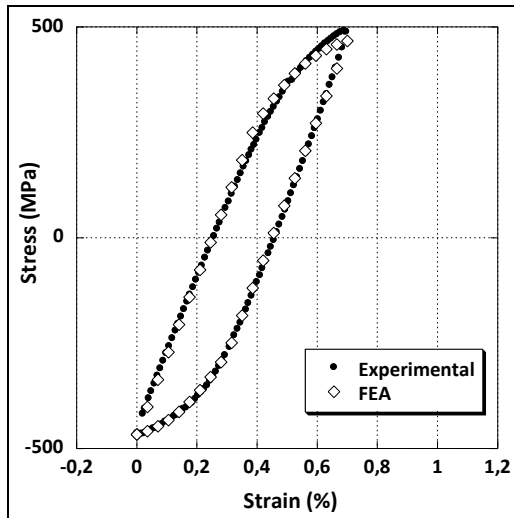
Fig.14. Comparison of experimental and modelled hysteresis curves for $\Delta\varepsilon_t$=0.7%
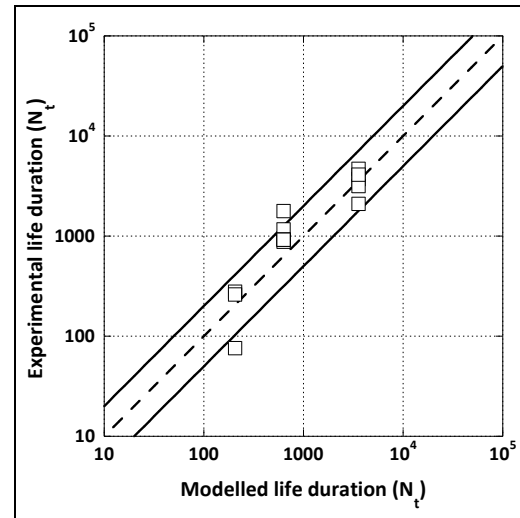

Fig.15. Comparison between experimental and modelled fatigue life of smooth samples

3.2.2. Life estimation on notched samples

The next step is to validate this model on a more complex geometry. Therefore, a "defect", in the present case a notch, is introduced in the rectangle which will introduce multiaxial stress and strain. FEA was conducted on geometry similar to the useful area of the experimental notched samples. The maximum strain is evaluated from FEA results and is used to predict the fatigue life from the Manson-Coffin relation generated from fatigue tests on smooth samples. The results are compared in fig. 16 and the error is less than 20%. Thus the method is also validated for complex geometry.
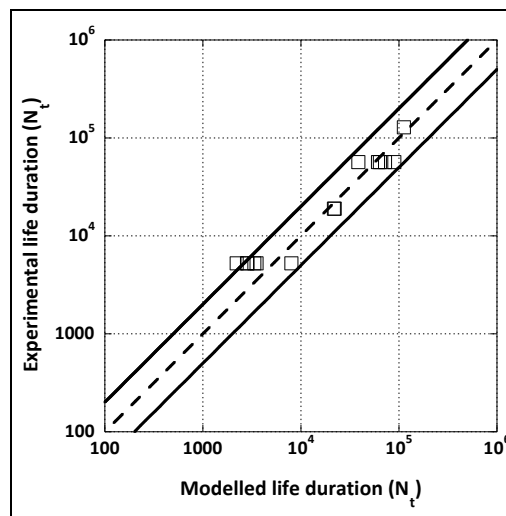

Fig.16. Comparison between experimental and modelled fatigue life of notched samples

3.3. Knowledge transfer for rotor design improvement

As pointed out in the introduction, the present rotors do not suffer from fatigue damage because of their oversizing. Especially, in the case of laminated rotors, the electrical steel sheets though they are very thin do not

break. An example of a patented laminated rotor is given in fig. 17 from which one can appreciate the complexity of the geometry. As well, one can notice that the shape of the sheet (in white in the figure) includes angular parts which can generate multiaxial stress and strain. At present time, rotor prototypes are designed by Valeo but their drawing cannot be included in the text for reason of confidentiality. The knowledge of the fatigue behaviour of the Fe3Si steel has been used to obtained improvement of two rotors. For rotor A, the electrotechnic performance (i.e. the torque value) of the machine should be increased keeping the same magnet mass. For rotor B, weighting of magnet is requested at iso-torque value.

To reach these goals, it is shown that magnetic saturation of the electrical steel should be obtained as easily as possible with the smallest size of the steel sheet. For that, the width of the part H in the drawing should be increase while the width of the part E should be decreased without changing the internal and external radii.

The tensile load considered in the calculation results from the rotation of the rotor which speed is 20 000 RPM. The critical part is the part E for which excessive or progressive elongation would appear as a problem. By FEA in which the values determined experimentally have been introduced, large plastic deformation is expected at the first cycle and then a cyclic stabilized state is quickly reached. Fig. 18 shows the cyclic stress-strain evolution during the stabilized state characterized by an elastic response. The simulated response is in agreement with the LCF behaviour. Indeed, the cyclic hardening observed during the LCF test at high strain range on the one hand and a quasi-stabilized evolution of the stress obtained at low strain range on the other hand allows considering no further elongation of the part E under cyclic load.

It is important to control the elongation at the starting period because the airgap between the rotor and the stator must not be filled. It is also important that the cyclic load does not lead to localized plasticity. Here, due to the low strain value, isolated dislocations displayed in their slip plane are expected and no evolution or transformation into other dislocations structures will occur.

Based on this, the reduction of the dimension of part E and the increase of the dimension of part H resulted in an increase of the torque value by 3% for rotor A and a reduction of the magnet mass by 8% for rotor B with reliable service conditions. The new drawing being under consideration for patenting cannot be presented.
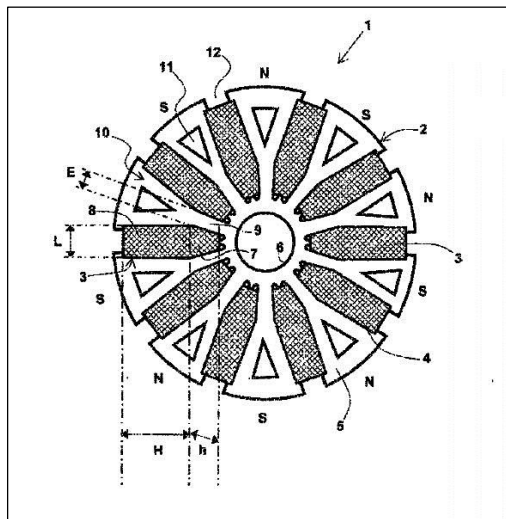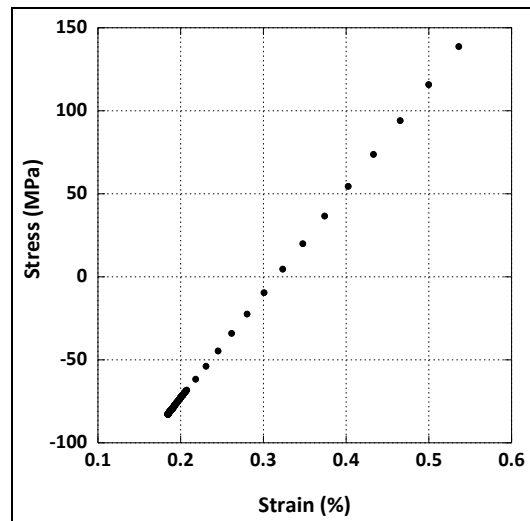

Fig.17. Laminated rotor from Valeo patent [6]

Fig.18. cyclic stress/strain state

4. Conclusion

The current work aimed at modifying the rotor geometry to improve the alternator performance. For that purpose, it was first necessary to document the fatigue behaviour of the material. Experimental tests were conducted on the Fe-3Si steel, it showed that this material hardens under cyclic loadings. TEM observations revealed unusual damage mechanisms with two different strain accommodations whether the steel is loaded in the high or low strain variation

regime. A fatigue resistance law is defined from the experimental LCF tests as well as the material parameters needed for FEA. The FEA results are validated on smooth and notch samples. Finally, the rotor design is modified which enables a light-weighting of the magnet or an increase of the torque value depending on the considered rotor and purpose.

References

[1] L. Vandenbossche, S. Jacobs, D. Van Hoecke, B. Weber, E. Leunis, E. Attrazic, Imrpoved iron loss modelling appraoch for advanced electric steels operating at high frequencies and high inductions in automotive machines, IEEE, 2012.

[2] H. Mughrabi, K. Herz et X. Stark, Cyclic deformation and fatigue behaviour of a-iron mono and polycrystals, International Journal of fracture 17, (1981) 193-220.

[3] C. Schayes, J.-B. Vogt, J. Bouquerel, F. Palleschi, S. Zaefferer, Cyclic plasticity mechanism of the M330-35A steel, to be published.

[4] C. Schayes, J. Bouquerel, J.-B. Vogt, F. Palleschi, S. Zaefferer, An EBSD investigation of Fe-3Si steel subjected to cyclic loading, to be published.

[5] J. Lemaitre, J.-L. Chaboche, Mechanics of solid materials, Cambridge University Press, 1994.

[6] J. Legranger, J.-C. Matt, L. Bouarroudj, F. Palleschi, Rotor de machine électrique tournanate et machine électrique tournante comprenant un rotor , demande de brevet d'invention, FR 2 982 093 – A1, 2011.